Improved correlation for elastic modulus prediction of metallic materials in the Small Punch Test

José Calaf Chica[(1)], Pedro Miguel Bravo Díez[(2)], Mónica Preciado Calzada[(3)]

E-mails: (1) Corresponding author, jcc0087@alu.ubu.es ; (2) pmbravo@ubu.es; (3) mpreciado@ubu.es
Postal address: Civil Engineering Department, University of Burgos, Avenida Cantabria s/n, 09006 Burgos, Spain

ABSTRACT

Generally, the correlation factors of parameters obtained from the load-displacement curve of small punch tests and the mechanical properties of materials are only acceptable for the materials tested in each investigation. Although the standardization of the correlation factors for different groups of materials is the objective in much of the research on the Small Punch Test (SPT), there are not many studies focused on the physical sense of these correlation factors. Consequently, the applicability of these factors needs the prior knowledge of the material to be tested with comparisons between SPT's and standardized tensile tests.

This investigation, through finite element modeling and a theoretical analysis, goes in depth into the understanding of the first zone of the SPT curve and the study of an unloading/loading cycle introduced into this zone in order to obtain an improved correlation factor for the elastic modulus. This factor is acceptable for most isotropic and homogeneous metallic alloys and depends only on the geometrical setup of the test. Experimental tests (tensile tests and SPT's) were added to these numerical/theoretical analyses to demonstrate the suitability of this correlation.

Keywords: Small Punch Test, SPT, Elastic Modulus, indentation, bending plate.

Note: This article did not receive any specific grant from funding agencies in the public, commercial, or non-profit sectors.

1 Introduction

The Small Punch Test (SPT) is a characterization test method widely studied in the recent decades. It consists of a punch which deforms a firmly gripped specimen (diameter ≥ 8 mm) between two dies until fracture (see Fig. 1). Many researchers have used the SPT to study the mechanical properties of different materials: elastic modulus, yield stress and tensile strength [1-2], ductile-brittle transition [3], fracture properties [4-7], etc. The interest in the SPT compared with standard tests is the smaller size, simpler geometry and cheaper manufacturing process of SPT specimens. Of these three points, the small size of the specimen was the main reason to develop this test method in the early 1980's to identify the loss of mechanical properties in metallic materials due to irradiation embrittlement [8-9].

During the test, load and displacement of the punch are recorded to obtain a load-displacement curve (see Fig. 2). Five main zones are distinguished in this curve [10]:

Zone I: elastic bending.
Zone II: transition between elastic and plastic bending.
Zone III: plastic hardening.
Zone IV: softening due to material damage initiation.
Zone V: crack growth with a circular shape around the center of the specimen until failure.

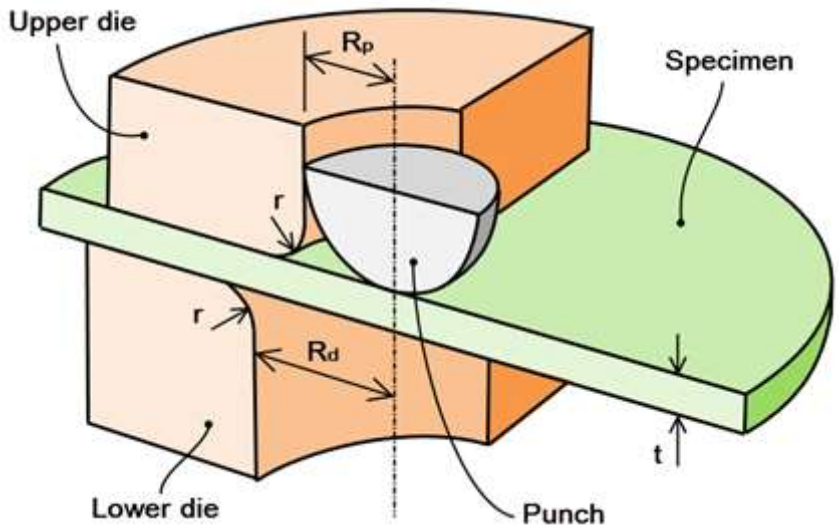

Fig. 1. Small punch test geometry

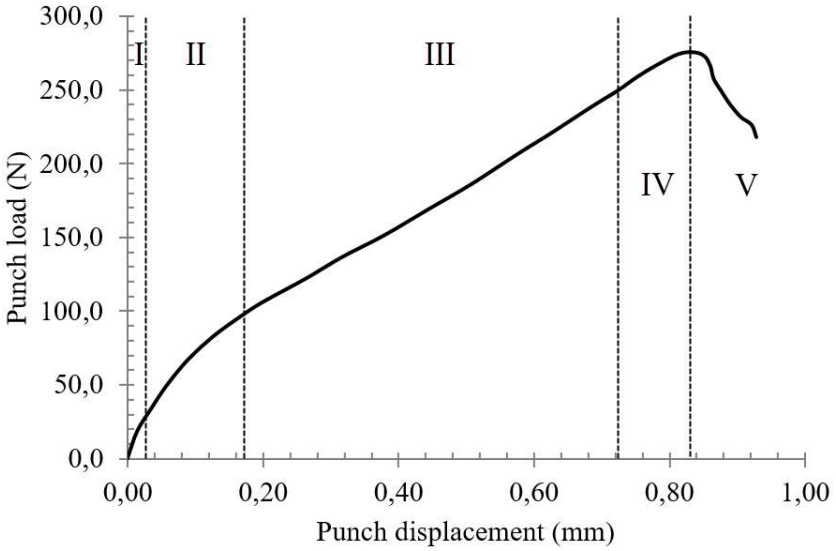

Fig. 2. Main behavior zones in the SPT curve

Different data are extracted from the SPT curve: "yield load" P_y, maximum load P_m, punch displacement at maximum load u_m and initial slope in zone I $Slope_{ini}$. They are correlated with mechanical properties obtained previously with standard tensile tests (Fig. 3 shows and example of SPT data extraction from load vs. displacement curve) [11]. The most well-known research about all these methods of correlation was that conducted by Mao and Takahashi [4], in which the yield strength σ_y was correlated with the "yield load" P_y (Fig. 3 shows an example of P_y extraction using the Mao method) with the following empirical equation (1):

$$\sigma_y = \alpha_1 \cdot \frac{P_y}{t^2} + \alpha_2 \qquad (1)$$

where t represents the thickness of the specimen and α_1 and α_2 are the correlation factors which are obtained from a regression analysis of the test results of the different materials or treatments to be correlated.

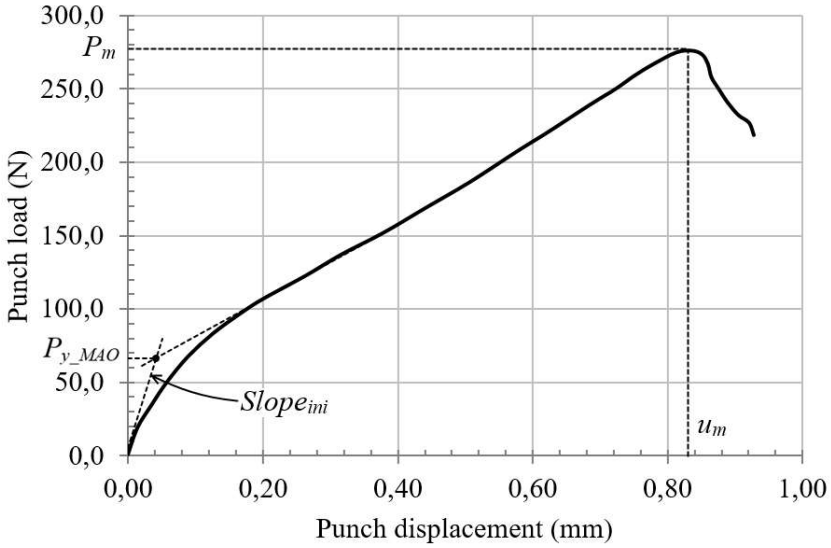

Fig. 3. Data extracted from SPT curve

Other parameters obtained from a standard tensile test (the elastic modulus E, the maximum stress σ_m and the strain ε_m for this maximum stress) were correlated using equations similar to the one used to correlate the yield stress σ_y [12]. Equations of these relationships are shown below (2, 3, 4):

$$\sigma_m = \beta \cdot \frac{P_m}{t^2} \quad (2)$$

$$\varepsilon_m = \varphi \cdot \frac{u_m}{t} \quad (3)$$

$$E = \lambda \cdot \frac{Slope_{ini}}{t} \quad (4)$$

García et al [11] made a σ_y vs. P_{y_MAO}/t^2 correlation with a wide set of metallic materials obtaining the correlation factors: $\alpha_1 = 0.442$ and $\alpha_2 = 0$. The deviation of experimental data with respect to the correlation equation reached values of about 22% in some of the tested materials (i.e. automobile dual phase sheet DP2)
Thus, material properties obtained from SPT correlation curves show a high level of deviation when a wide set of materials is considered. The causes of these high deviations might be:

a) Small deviations in the SPT specimen geometry. This type of miniature test needs a high level of precision in thickness tolerance of the specimen (from 0.495 mm to 0.505 mm).
b) Deviations in the setup of the specimen and the upper and lower dies: initial gaps, non-uniform contact pressure between parts, etc.
c) Dependency of data extracted from the SPT curve on more than one mechanical property. This problem could be solved with a search of other data from an SPT curve whose dependency on the material mechanical properties is strong enough with only one of these properties and much less important with the others.

Points (a) and (b) may be solved testing a set of SPT specimens made of the same material and checking the repeatability of all SPT curves. When deviations between the SPT curves result negligible, the setup is considered adjusted and the causes of deviations are reduced to the previous point (c).

In this paper, the third point was analyzed to obtain a correlation for the elastic modulus by means of:

a) The analysis of the strong dependency of $Slope_{ini}$ obtained from the SPT curve with more than one mechanical property.

b) The search for an alternative method to correlate the SPT curve data with the elastic modulus E of the tested material. New data were extracted from the SPT curve searching for a high level of dependency on the elastic modulus and a very low dependency on the other mechanical properties of the material.

2 Methodology and materials

As presented in the introductory section, the first slope of the SPT curve ($Slope_{ini}$; see Fig. 3), understood as an elastic zone of the SPT test (the zone I of Fig. 2), can be correlated with the elastic modulus E using Eq. 4.

The real behavior of elastic zone I has been studied by some researchers, and it shows a combination of two modes of deformation: plastic indentation of the punch in the specimen and elastic bending deformation due to the deflection of the specimen [13]. Thus, the slope of this elastic zone I of the SPT curve could be a combination of two different rigidities: an elastic stiffness due to the specimen deflection and a variable plastic stiffness of the punch indentation in the specimen. This combination results in a lower rigidity than pure elastic bending and in a lower slope in the SPT curve. So, the slope of this initial "elastic" zone depends on the plastic behavior of the tested material and, therefore, two materials with the same elastic modulus E and different yield strength σ_y, maximum stress σ_m and strain ε_m should show an "elastic" zone I with a different slope ($Slope_{ini}$).

Therefore, the $Slope_{ini}$ is not a good SPT parameter to be correlated with the elastic modulus E, because it is dependent on elastic and plastic properties. This could be the reason why correlation factors between elastic modulus E and $Slope_{ini}$ for some materials does not match with other materials.

Researchers performed detailed FEM analyses to evaluate the behavior of the SPT specimens at different punch displacements where punch load values were extracted to be correlated with material mechanical properties [14-15]. These studies verified the arbitrary character of the different definitions and criteria of some of these correlations [16].

Firstly, the $Slope_{ini}$ was analyzed to see how high a level of deviation there was when it was correlated with the elastic modulus. In addition, a search for new data extracted from the SPT curve showing a nearly pure elastic behavior was performed. The following analyses were performed:

a) Simulations of SPT with Abaqus FE software with eight different hypothetical materials (M1 to M8) were performed. Some unloading/loading cycles (UL cycles) were included into Zones II and III of all these analyses (Fig. 4 shows an example of a load-displacement curve obtained from these FEM simulations). During this UL cycle, no significant plastic behavior was generated, so its slope ($Slope_{UL}$) represents nearly pure elastic behavior. A study of the Poisson ratio influence in the slope of the previous UL cycles was also performed to guarantee a low dependency of $Slope_{UL}$ on this elastic property.

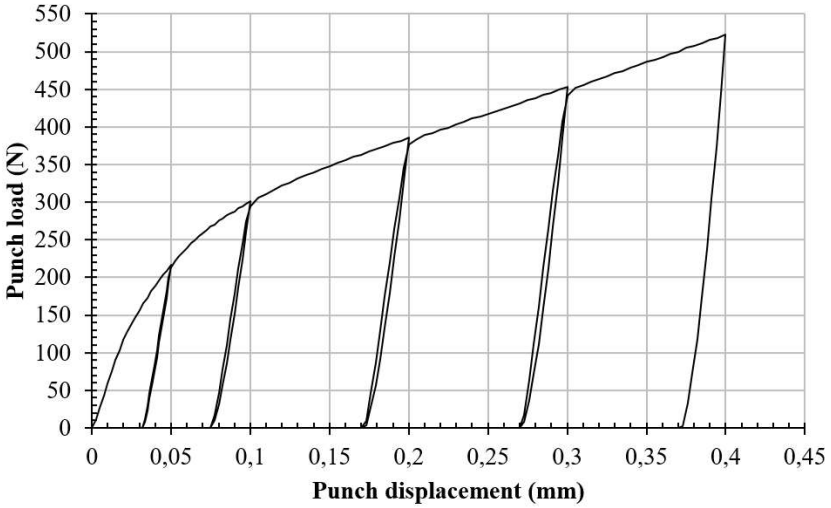

Fig. 4. FEM simulation of SPT test with UL cycles

b) A theoretical study with analytical equations of contact mechanics and plate bending was performed to evaluate the different dependencies of the $Slope_{UL}$ parameter on more than one mechanical property.
c) The $Slope_{ini}$ and the $Slope_{UL}$ obtained from eight previous hypothetical materials were correlated with the elastic modulus E introduced in each FE model and deviations of both correlations were obtained and compared.

In FEM simulations, the specimen thickness was set at 0.5 mm. The rest of the geometric parameters were: $R_d = 2.0$ mm, $R_p = 1.25$ mm and $r = 0.5$ mm (see Fig. 1).

The mechanical properties of hypothetical materials M1 to M8 are shown in Table 1. Three values for the Poisson ratio were selected (υ = {0.25, 0.30 and 0.35}), and the eight materials were studied in this range. The plastic behavior for all materials was performed with an isotropic-kinematic hardening model following a Ramberg-Osgood equation (see Equations 7 and 8 [17]):

$$\varepsilon = \frac{\sigma}{E} + \varepsilon_{offset}\left(\frac{\sigma}{\sigma_y}\right)^n \qquad (7)$$

$$n = \frac{\ln\left(\dfrac{\varepsilon_m - {}^{\sigma_m}/_{E}}{\varepsilon_{offset}}\right)}{\ln\left(\dfrac{\sigma_m}{\sigma_y}\right)} \qquad (8)$$

where $\varepsilon_{offset} = 0.002$ is the offset strain used to calculate the yield strength.

Material	E (MPa)	ν	σ_y (MPa)	σ_m (MPa)	ε_m (mm/mm)	n*
M1	50000	0.30	100	200	0.20	6.61
M2	50000	0.30	200	300	0.10	9.50
M3	100000	0.30	200	350	0.25	8.60
M4	100000	0.30	350	450	0.20	18.23
M5	200000	0.30	400	650	0.20	9.45
M6	200000	0.30	1000	1300	0.15	16.29
M7	400000	0.30	2000	2500	0.20	20.50
M8	400000	0.30	2500	2600	0.10	98.03
F1110	216430	0.30	550.6	615.6	0.086	-
F1140	204910	0.30	745.25	922.67	0.0572	-
Al 6061 T6	65617	0.33	186.74	272.21	0.1794	-
Mg AZ31	42889	0.35	137.72	262.44	0.1623	-
15-5 PH H900	194926	0.30	1215	1310	0.1615	-
Cu C18070	128234	0.34	564.4	577.4	0.0119	-

(*) Ramberg-Osgood parameter

Table 1. Mechanical properties of the hypothetical and the experimental materials

Secondly, experimental tests (standard tensile tests in accordance with ASTM E8M and small punch tests) were performed to verify all previous numerical and theoretical results. Two carbon steels (F1110 and F1140), an aluminum alloy 6061 T6, a 15-5PH H900 steel, a magnesium alloy AZ31, and a copper alloy C18070 were tested (one SPT and one tensile test were considered for each material). FEM analysis of one of these SPT's was also performed to demonstrate the similarity and confidence of the numerical model. In this FEM study, material

behavior was simulated with a tabulated representation of stress-strain data obtained from the standard tensile test. Mechanical properties of the six tested materials are shown in Table 1.

Displacement data recorded in the experimental SPT were obtained from an extensometer, which measures the movement of the punch assembly. The stiffness of different parts of this punch assembly was subtracted using a calibration test. So in this paper, experimental SPT curves represent the displacement of the specimen upper face.

3 Numerical and theoretical analyses

The small punch test was simulated by means of an implicit analysis with Abaqus software using an axisymmetric model. Punch and upper and lower dies were taken as analytically rigid bodies. The global mesh size of the specimen was equal to 0.025 mm and was made up of quadrilateral elements with reduced integration and hourglass control (CAX4R). Contacts between the different parts were simulated with a friction coefficient $\mu = 0.18$ (the typical value used for steel-steel contact without lubrication). The material properties used in these simulations are listed in Table 1.

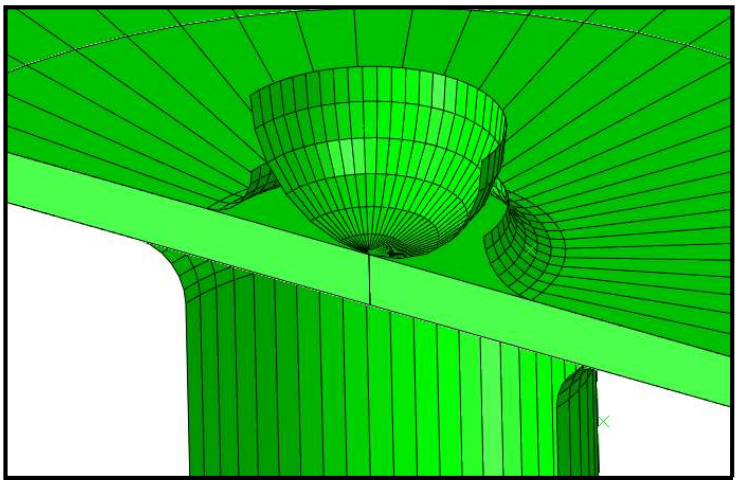

Fig. 5. SPT FE model

3.1 $Slope_{ini}$ analysis

Fig. 6 shows the behavior of the specimen in FEM simulation with material M5 at different displacements of the punch in zones I and II. The grey areas in the simulation represent regions where yield strength is surpassed.

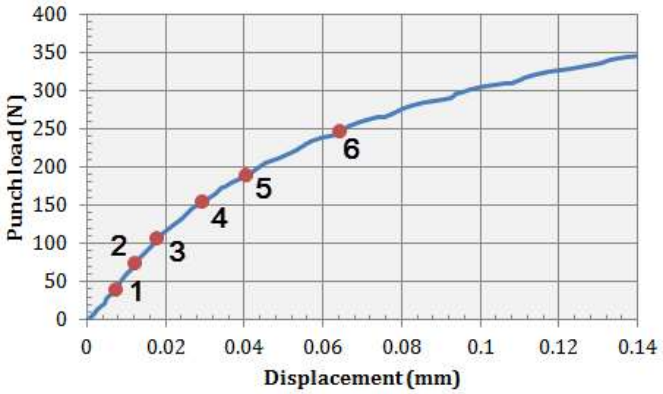

Fig. 6. Yielding in zones I and II in SPT simulation for M5 material

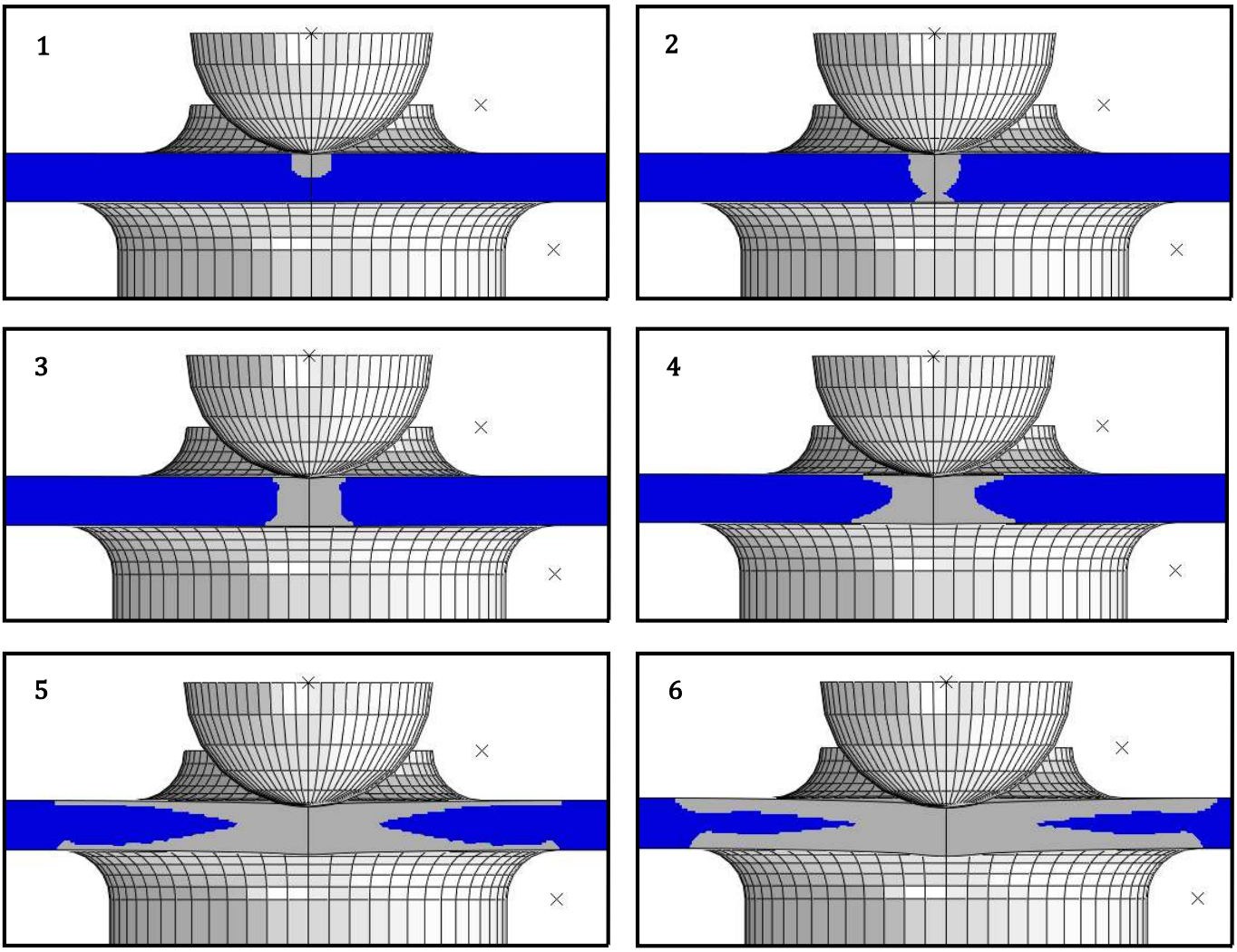

Fig. 6 (cont.). Yielding in zones I and II in SPT simulation for M5 material

In the first zone of the SPT, a plastic area grows just below the punch reaching the thickness of the specimen, and after that, it expands along the upper and lower surfaces of the tested specimen towards the outer perimeter. The displacement in zone I of the SPT curve coincides with the sum of the elastic bending of the specimen and the local plastic indentation.

When the plastic indentation affects the entire thickness of the specimen and expands over sufficient area, the slope of the SPT curve begins to change (point 3 in Fig. 6). After point 3, a new stiffness factor appears: the plastic bending of the specimen. The percentage of punch displacement due to this plastic bending grows as the percentage of displacement due to elastic bending decreases with loading.

When plastic bending dominates the punch movement and elastic bending is negligible, the slope of the SPT curve stabilizes. At this point, the first stages of zone III of the SPT curve are reached.

After this detailed study of zones I and II of the SPT curve, zone I clearly shows that stiffness is influenced by the combination of elastic bending and plastic indentation. So, this $Slope_{ini}$ of the SPT curve, which is the graphical representation of specimen stiffness, does not seem to be the best way to obtain the elastic modulus E.

3.2 Hypothetical material analysis

Eight hypothetical materials M1 to M8 (see Table 1 for the mechanical properties of these materials) were simulated with the same FE model used in the previous section. Fig. 7 represents the load-displacement SPT curves for all of these hypothetical materials with UL cycles introduced during the test simulation. Four complete UL cycles, with

unloading and loading steps, were established at different initial punch displacements: 0.05, 0.10, 0.20, and 0.30 mm. The last cycle, at a punch displacement of 0.40 mm, terminated after the unloading step of the UL cycle.

Hysteresis was observed in the UL cycles, as shown in Fig. 7. It is produced by the yielding generated by the residual stresses, combined with the contact nonlinearities in the punch and upper face of the specimen. Fig. 8 shows a detailed view of the UL cycle initiated at a punch displacement of 0.1 mm for the material M1. In this figure, the nonlinearities are more evident near the maximum and minimum displacements of the UL cycle.

Fig. 9 shows the slope of the SPT curve in the UL cycle initiated at 0.1 mm for the material M1. The slope was calculated from the first derivative of the equations of two order 5 polynomial regressions fitted to the two zones of the UL cycle. The UL cycle is divided into two steps: the unloading step (blue curve) and the loading step (red curve). Arrows are plotted in both steps of Fig. 9 to show the direction of the UL cycle: the unloading step goes from A to B1; the transition from unloading to loading steps shows a jump from B1 to B2; and the loading step goes from B2 to C, where the UL cycle is finished. The loading step shows a wider part with a stabilized slope centered in the middle of the step. Thus, $Slope_{UL}$ is calculated as follows:

1. The punch displacement increment (see Fig. 8) is the difference between the maximum and minimum punch displacements in the UL cycle. The minimum displacement value is the first which reaches the minimum punch load in the UL cycle.
2. $Slope_{UL}$ is the slope of the linear regression of the loading step (thick black line in Fig. 9) performed between the 20% and 80% of the punch displacement increment. An example of linear regression for UL cycle initiated at 0.1 mm of material M1 is shown in Fig.8 and Fig. 9.

Although Fig. 8 and 9 only represent the behavior of the material M1, all hypothetical materials showed a similar behavior in the UL cycles.

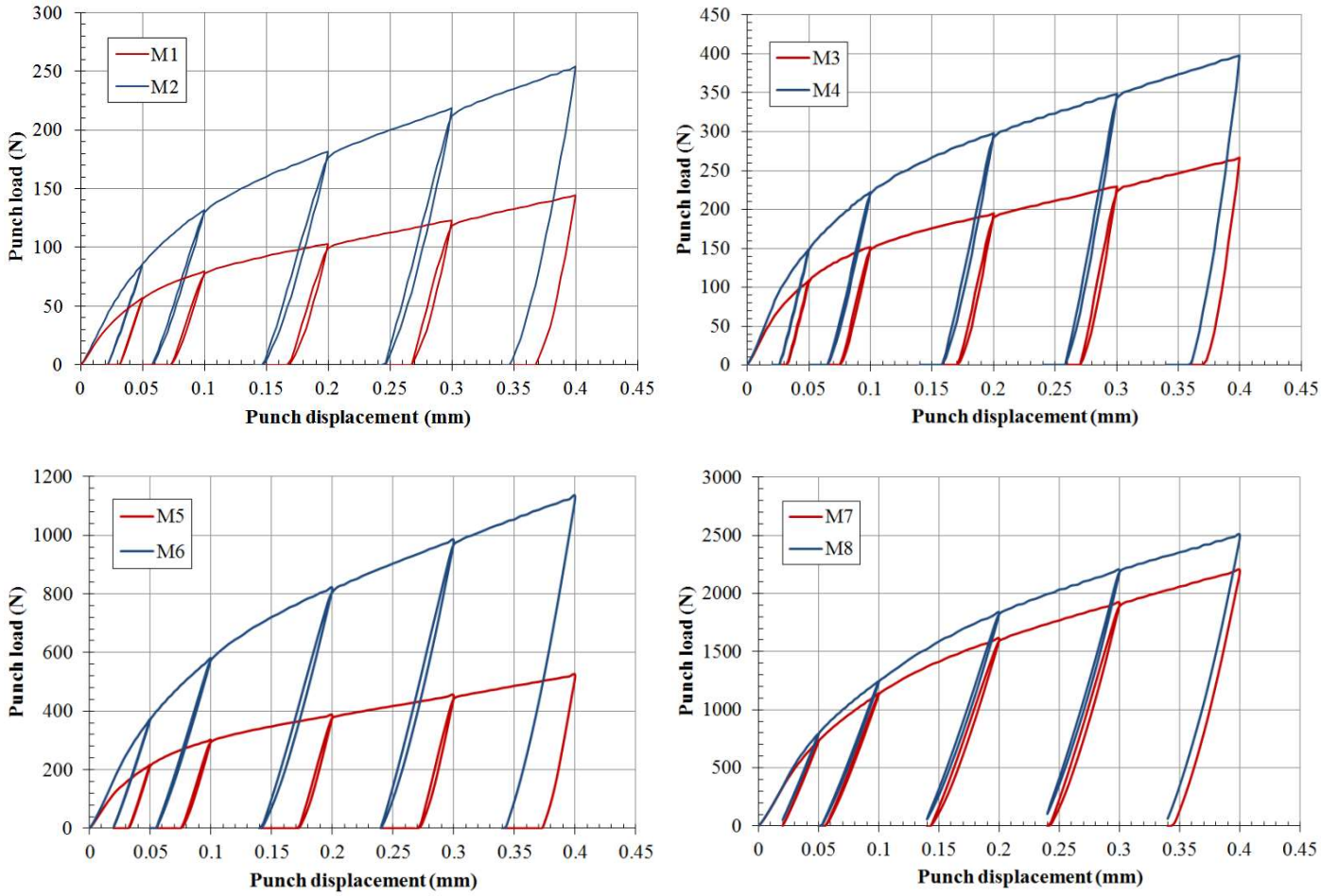

Fig. 7. SPT curves for simulated materials with UL cycles

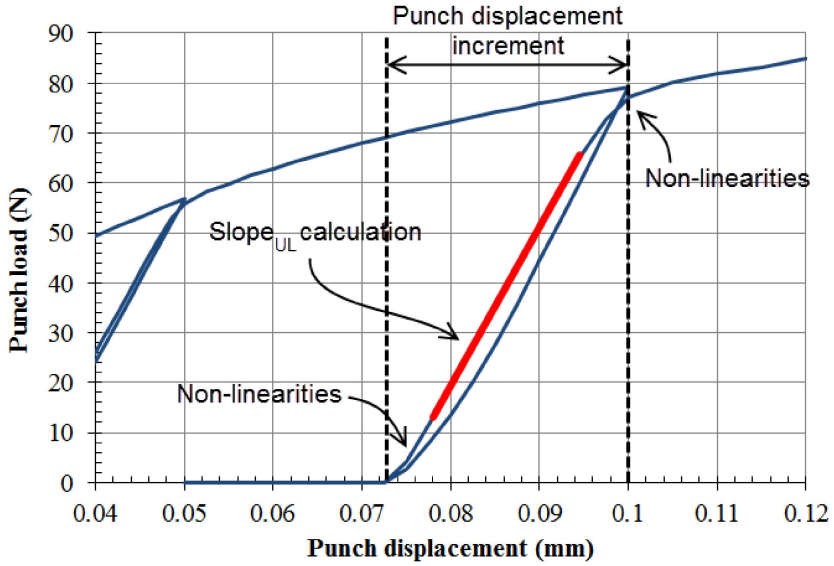

Fig. 8. Detail of the UL cycle initiated at 0.1 mm for material M1

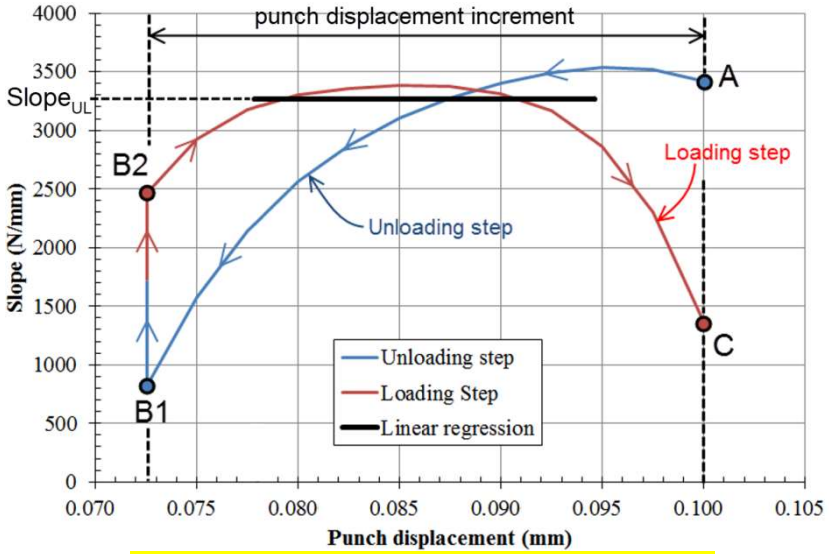

Fig. 9. Slope of the UL cycle for material M1

Zone I of the SPT curve shows non-linear behavior (see Fig. 2), thus the $Slope_{ini}$ was obtained from the maximum slope of zone I. A 5th order polynomial regression of SPT curve data, from 0.00 mm to 0.05 mm of punch displacement, was adjusted in all materials to obtain the maximum slope of zone I. This procedure was applied to all hypothetical materials. Table 2 shows the obtained $Slope_{ini}$ and $Slope_{UL}$.

Hypothetical materials were designed in pairs with the same elastic modulus: (M1,M2), (M3,M4), (M5,M6) and (M7,M8). These pairs showed a similar $Slope_{UL}$ and a dissimilar $Slope_{ini}$, so correlation of the elastic modulus with the $Slope_{UL}$ appears to be more precise. Fig. 10 shows the improvement in accuracy of the correlation with the elastic modulus obtained with $Slope_{UL}$. It should be noted that the correlation factor between $Slope_{UL}$ and the elastic modulus depends on the punch displacement where the unloading/loading cycle was initiated. This dependency is analyzed and shown in subsection 3.4 of this article.

		Slope$_{UL}$ (N/mm)				Slope$_{ini}$ (N/mm)
	Unloading position (mm)	0.05	0.1	0.2	0.3	N/A
Hypothetical materials	M1	3148.4	3264.1	3615.4	4136.5	1614.4
	M2	3148.2	3326.8	3641.5	4152.1	2164.1
	M3	6434.3	6663.4	7228.4	8364.4	3220.4
	M4	6388.3	6858.1	7612.1	8790.1	3983.7
	M5	12883	13428	14690	16823	6481.4
	M6	12474	13378	14882	17054	9184.3
	M7	25193	26984	29932	34500	18299.9
	M8	24993	26992	30279	35102	19277.3

Table 2. Slopes of SPT simulation for the hypothetical materials

To standardize the correlation method, the punch displacement for UL cycle initiation was fixed at 0.10 mm, obtaining a correlation factor of $\lambda_{UL\ 0.1} = 14.84\ mm^{-1}$ (see Fig. 10). Although this setting of the punch displacement for UL cycle initiation does not guarantee the same local stress and deformation of the specimen, the slope of the UL cycle at 0.10 mm shows a good linear correlation with the elastic modulus with negligible deviations (R^2=0.9999).

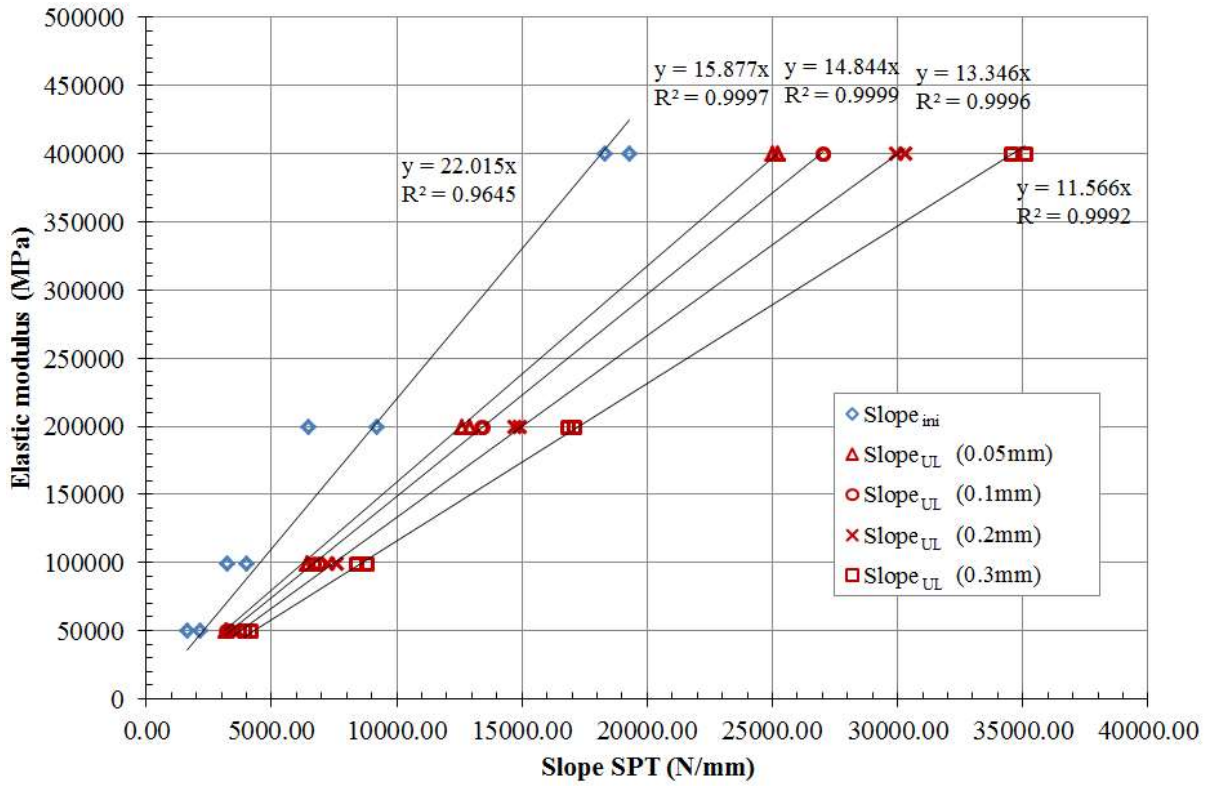

Fig. 10. Elastic modulus correlation with *Slope$_{ini}$* and *Slope$_{UL}$*

3.3 Analysis of the Poisson ratio influence

The materials analyzed in the previous section had the same Poisson ratio. This elastic property should affect the slope of the SPT load-displacement curve, so another FEM study was carried out to show the influence of the Poisson ratio in the *Slope$_{UL_0.1}$* correlation with the elastic modulus. This study was focused on metallic alloys used in assemblies with substantial mechanical requirements. A revision of pressure vessel and aeronautics material codes [18,19] was performed to delimit a range for the Poisson ratio. The selected range {0.25, 0.30, 0.35} includes all metallic materials covered by these Codes.

Fig. 11 shows the elastic modulus E vs. $Slope_{UL\_0.1}$ the for the hypothetical materials M1 to M8 for the selected values of the Poisson ratio. A correlation factor value of $\lambda^{FEM}_{UL\_0.1} = 14.828\ mm^{-1}$ for the linear regression was obtained. Table 3 presents the $Slope_{UL\_0.1}$ for the hypothetical materials and the calculated elastic modulus obtained from Eq. 9.

$$E = \lambda^{FEM}_{UL\_0.1} \cdot Slope_{UL\_0.1} \qquad (9)$$

Table 4 shows a summary of deviations between the calculated elastic modulus and the introduced elastic modulus in the FEM simulations. A maximum deviation of 4.77% ensured a low influence of the Poisson ratio in the $Slope_{UL}$ and a high reliability of this correlation method for a wide selection of structural materials.

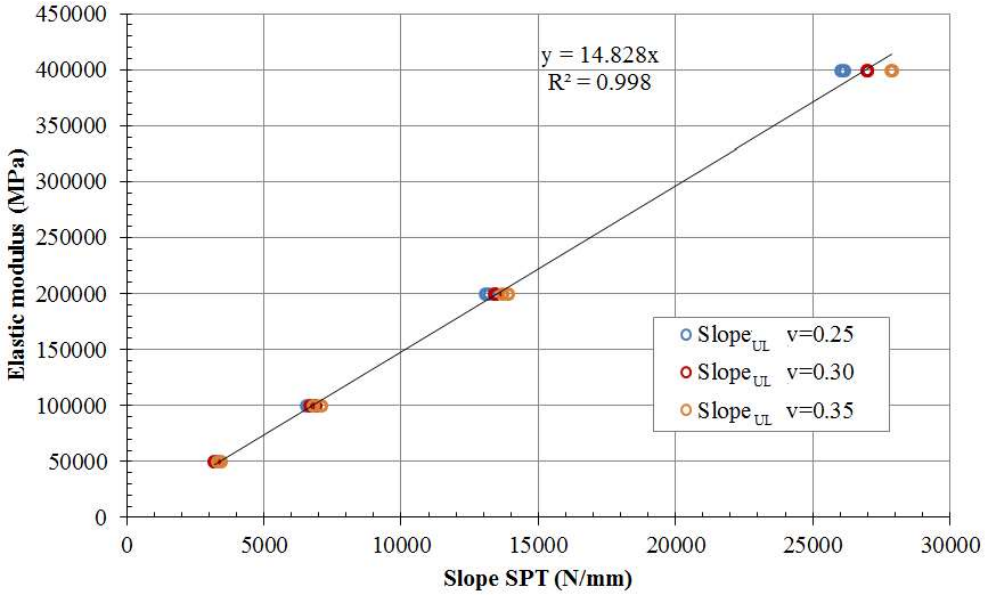

Fig. 11. Elastic modulus vs. $Slope_{UL}$ for the different Poisson ratio values

	$Slope_{UL}$ (N/mm)			Calculated Elastic modulus (MPa)		
	ν = 0.25	ν = 0.30	ν = 0.35	ν = 0.25	ν = 0.30	ν = 0.35
M1	3230.8	3264.1	3377.9	47906.3	48400.1	50087.5
M2	3248.0	3326.8	3424.6	48161.3	49329.8	50780.0
M3	6555.0	6663.4	6809.7	97197.5	98804.9	100974.2
M4	6701.5	6858.1	7065.6	99369.8	101691.9	104768.7
M5	13172.0	13428.0	13687.0	195314.4	199110.4	202950.8
M6	13046.0	13378.0	13885.0	193446.1	198369.0	205886.8
M7	26156.0	26984.0	27845.0	387841.2	400118.8	412885.7
M8	26012.0	26992.0	27888.0	385705.9	400237.4	413523.3

Table 3. Poisson ratio influence in calculated Elastic Modulus

	Elastic modulus deviation (%)		
	ν = 0.25	ν = 0.30	ν = 0.35
M1	4.19	3.20	-0.18
M2	3.68	1.34	-1.56
M3	2.80	1.20	-0.97
M4	0.63	-1.69	-4.77
M5	2.34	0.44	-1.48
M6	3.28	0.82	-2.94
M7	3.04	-0.03	-3.22
M8	3.57	-0.06	-3.38

Table 4. Calculated elastic modulus deviation from FEM elastic modulus

3.4 Theoretical analysis

The small punch test is a mechanical test which combines indentation and plate bending. The UL cycles analyzed previously show an elastic behavior which could be studied as a simplified circular plate clamped along the outer perimeter and punched by a point load in the center. The elastic plate bending for this situation is represented by Equation 10 [20]:

$$P = \frac{4\pi E t^3}{3a^2(1-v^2)}\delta \qquad (10)$$

where:
a, plate radius,
P, concentrated load,
E, elastic modulus,
t, plate thickness,
v, Poisson ratio,
δ, plate center deflection.

The theoretical plate bending behavior for material M1 is:

$$P_{M1} = \frac{4\pi E_{M1} t^3}{3a^2(1-v^2)}\delta_{M1} = 4600.7 \cdot \delta_{M1}$$

In Table 2, $Slope_{UL}$ showed values from 3148.4 N/mm to 4136.5 N/mm depending on the initial punch displacement point where the UL cycle was initiated, so a direct comparison between this theoretical equation and FEM results for material M1 showed an important deviation (from 11.2% to 46.1%).

The SPT shows some differences with the idealized circular clamped plate:

a) During the UL cycle, load is more concentrated in the outer radius of the circular contact surface between punch and plate instead of in the center of the plate (see Fig. 12).
b) Basic theoretical bending plate formulation neglects the deflection due to shear stress.
c) Elastic indentation is not considered in plate bending equations.

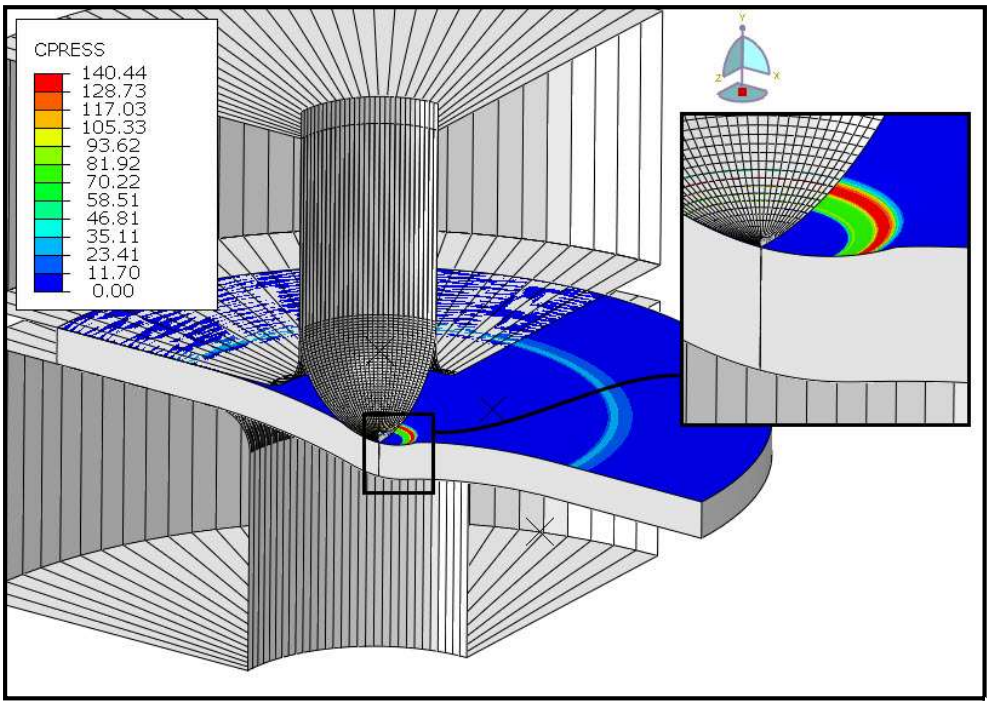

Fig. 12. Contact pressure (MPa) between punch and plate in FEM simulation

Equation 11 [21] considers a clamped circular plate with a uniformly distributed load along a concentric annulus (see fig. 13 for theoretical plate model).

$$\delta_{bending} = \frac{P}{8\pi D}\left[b^2 ln\left(\frac{b}{a}\right) + \frac{a^2 - b^2}{2}\right] \qquad (11)$$

where P is the punch load, a is the outer radius, b is the contact surface radius between punch and plate, and D is the flexural stiffness (see Eq. 12).

$$D = \frac{Et^3}{12\left(1 - \upsilon^2\right)} \qquad (12)$$

where E is the elastic modulus, t is the plate thickness, and υ is the Poisson ratio.

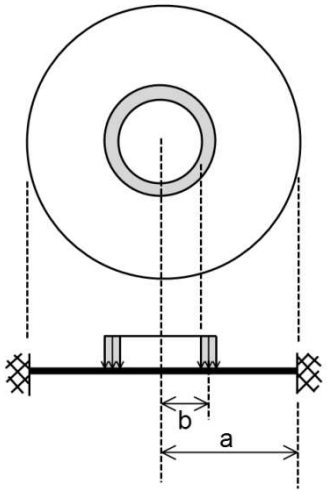

Fig. 13. Clamped circular plate with a uniformly distributed load along a concentric annulus

Deflection due to shear stress for the theoretical model shown in Fig. 13 was analyzed by Timoshenko et al. [20]:

$$\delta_{shear} = \frac{Pt^2}{8\pi D(1-\upsilon)}\ln\left(\frac{a}{b}\right) \qquad (13)$$

And finally, elastic indentation, which is recovered when the punch load is removed, can be estimated by Equation 14 [22]:

$$\delta_{indentation}^{2} = \frac{27\pi P\sigma_m\left(1-\upsilon^2\right)^2}{16E^2} \qquad (14)$$

where:
σ_m is the maximum stress of the material.

The original equation (14) [22] uses the elastic limit σ_y instead of σ_m, although that equation is based on an elastic-perfectly-plastic model, so taking into account the high level of plastic strain reached during SPT at the indentation zone, Von Mises stresses will reach values closer to σ_m than to σ_y.

Thus, the total elastic deflection during the UL cycle is equal to the sume of the three equations (11, 13 and 14):

$$\delta_{total} = \frac{P}{8\pi D}\left[b^2 ln\left(\frac{b}{a}\right) + \frac{a^2-b^2}{2}\right] + \frac{Pt^2}{8\pi D(1-\upsilon)}\ln\left(\frac{a}{b}\right) + \frac{1-\upsilon^2}{E}\sqrt{\frac{27\pi P\sigma_m}{16}} \qquad (15)$$

in which b and P were obtained from the FEM analyses when the punch displacement of each UL cycle was initiated (see Table 5).

		***b* (mm)**				***P* (N)**			
	Unloading position (mm)	0.05	0.10	0.20	0.30	0.05	0.10	0.20	0.30
Hypothetical materials	M1	0.240	0.310	0.410	0.490	56.90	83.56	103.10	123.23
	M2	0.217	0.301	0.420	0.519	85.99	131.86	181.34	218.32
	M3	0.247	0.321	0.430	0.508	109.26	151.77	194.67	229.67
	M4	0.237	0.331	0.450	0.538	149.58	222.69	298.26	348.77
	M5	0.247	0.331	0.449	0.527	218.71	305.57	397.82	469.19
	M6	0.217	0.302	0.430	0.529	372.81	579.49	820.86	982.96
	M7	0.217	0.312	0.440	0.529	735.61	1139.66	1612.29	1918.26
	M8	0.208	0.312	0.451	0.549	794.35	1243.12	1837.33	2199.96

Table 5. Radius of contact surface between punch and plate (b) and punch load (P) obtained from SPT simulation for the hypothetical materials.

Representing the punch load P_i at the maximum stress σ_m vs. the different punch displacements for the hypothetical materials M1 to M8 from data obtained in previous FEM simulations (see Fig. 14), P_i shows a linear dependency on the maximum stress σ_m with sufficient correspondence to consider the next relation (16).

$$\sigma_m^{Mj} = k_i P_i^{Mj} \quad i \in \{0.05;0.10;0.20;0.30\} \wedge j \in (1,8) \qquad (16)$$

where k_i is a factor mostly dependent on the punch displacement where the UL cycle is initiated and nearly independent of the material properties. Thus, if the punch displacement where the UL cycle is initiated is fixed for all tests, k_i can be considered as a constant value.

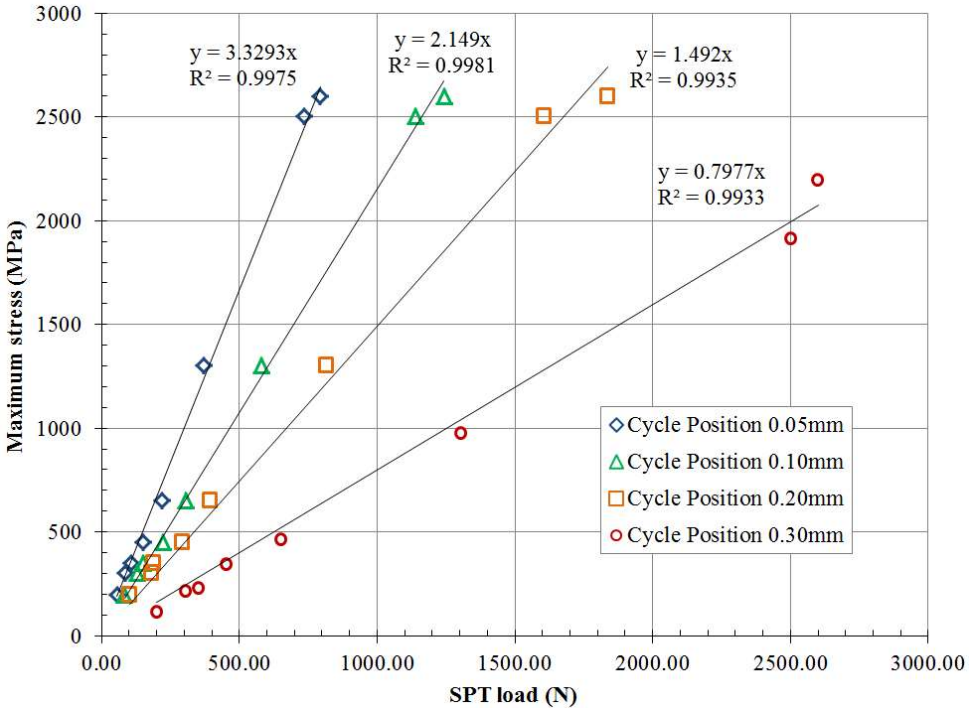

Fig. 14. Punch load P vs. maximum stress σ_m for each initial punch displacement where the UL cycle was initiated in FEM simulations

Fig. 15 shows that the radius of the contact surface b did not change significantly amongst the hypothetical materials M1 to M8 for the same punch displacement so, as seen previously with factor k_i, it is mostly dependent on punch displacement where the UL cycle is initiated and less dependent on material properties.

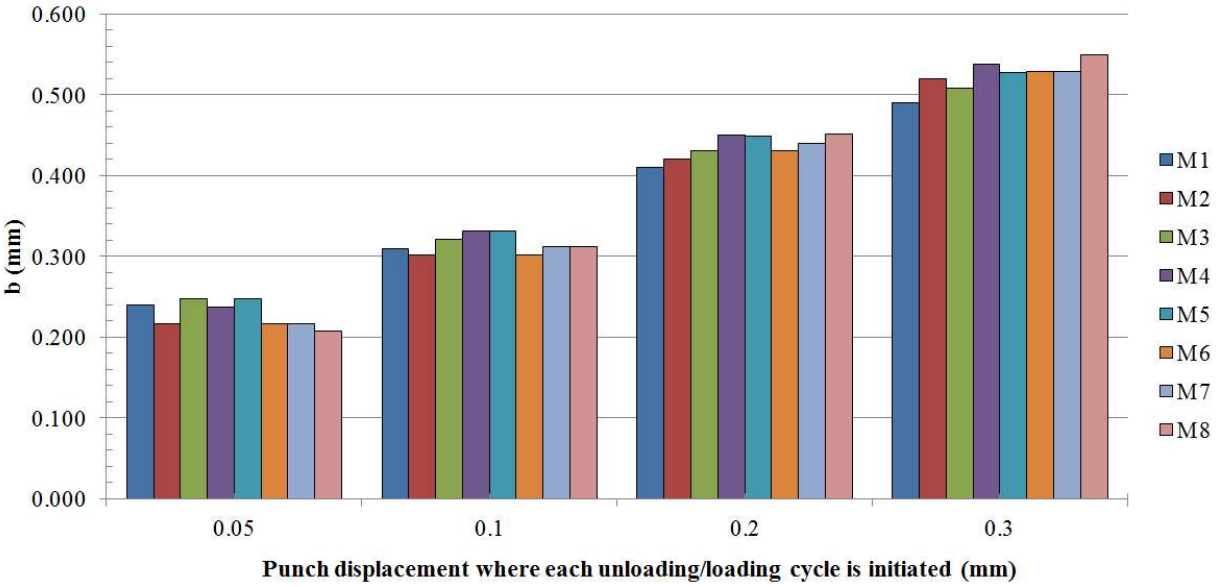

Fig. 15. Radius of the contact surface b vs. each initial punch displacement where the UL cycle is initiated for all hypothetical materials analyzed in FEM simulations

There are two reasons for the increment of $Slope_{UL}$ with the increment of punch displacement where the UL cycle is initiated. Firstly, the radius of the contact surface b increases with the increment of the unloading displacement

where the UL cycle is initiated and, as a consequence, $Slope_{UL}$ is increased. Secondly, the elastic indentation, which is recovered when the punch load is removed, increases the global rigidity (and the $Slope_{UL}$) of the theoretical model when the factor k_i is reduced with the increment of the punch displacement. As explained before, if the punch displacement where the UL cycle is initiated is fixed for all tests, k_i and b can be considered as constant values.

Combining equations (12), (15) and (16), theoretical $Slope_{UL}$ of the UL cycles is:

$$Slope_{UL} = \frac{P_i^{Mj}}{\delta_{total}} = \frac{E}{1-\upsilon^2}\left[\frac{3}{2\pi t^3}\left(b_i^2 ln\left(\frac{b_i}{a}\right) + \frac{a^2-b_i^2}{2}\right) + \frac{3}{2\pi t(1-\upsilon)}\ln\left(\frac{a}{b_i}\right) + \frac{3}{4}\sqrt{3\pi k_i}\right]^{-1} \quad (17)$$

Fig. 16 shows a comparison between $Slope_{UL}$ obtained numerically in the previous analyses and the $Slope_{UL}$ obtained from the theoretical equation (17). The accuracy of this theoretical model seems to be good enough to confirm the complexity of the SPT behavior during the UL cycle and to show the main cause for unload slope variation due to changes in punch displacement where the UL cycle is initiated.

Table 6 summarizes the k_i value and the averaged values of b_i for each unloading position. In the previous FEM study, UL cycles were standardized to an initial punch displacement of 0.1 mm, so replacing b_i and k_i for $b_{0.1}$ and $k_{0.1}$ from table 6 in equation (17) and substituting geometrical factors (t = 0.5 mm; a = 2.5 mm), the resultant equation is:

$$Slope_{UL\_0.1} = \frac{E}{1-\upsilon^2}\left[14.337 + \frac{1.978}{1-\upsilon}\right]^{-1} \quad (18)$$

In the next section, this theoretical equation (18) is analyzed and compared with experimental results.

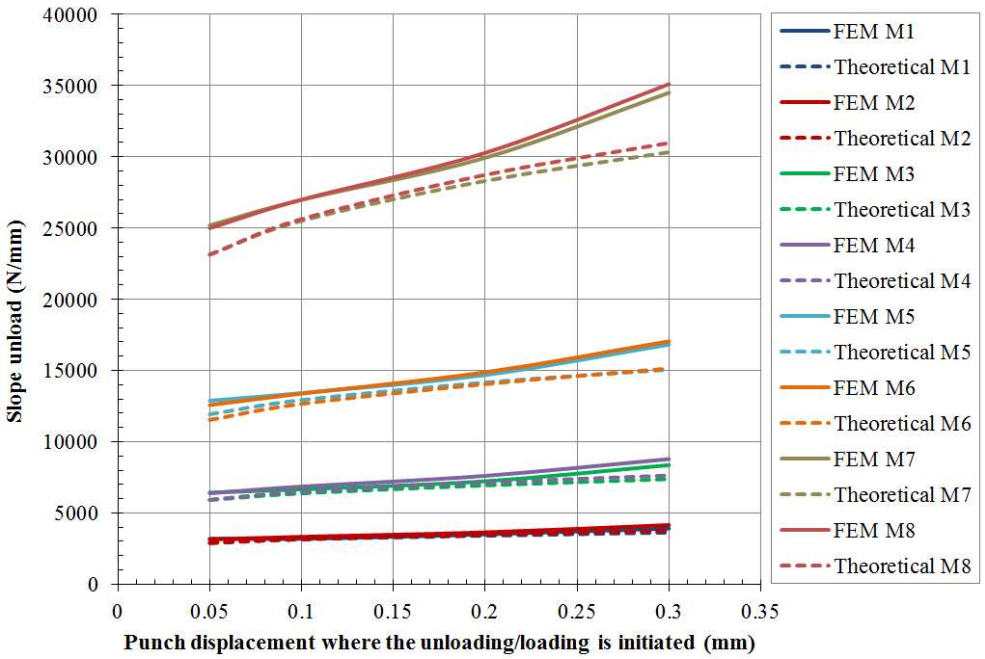

Fig. 16. FEM and theoretical slopes of the UL cycles vs. punch displacement where the UL cycle was initiated

Unloading position (mm)	0.05	0.10	0.20	0.30
$\mathbf{b_{averaged}}$ **(mm)**	0.229	0.315	0.435	0.524
$\boldsymbol{k}$ **(mm^{-2})**	3.329	2.149	1.492	0.798

Table 6. b_i and k_i values for different unloading positions

4 Experimental procedures and results

Six alloys, aluminum alloy 6061 T6, magnesium alloy AZ31, copper alloy C18070, and three steels, F1110, F1140 and 15-5PH H900 were tested using standard tensile tests (ASTM E8M) and small punch tests to verify the numerical results previously shown.

Table 1 shows the mechanical properties for all tested materials and Figure 17 represents the stress-strain curve of the 15-5PH H900 tensile test. SPT FEM simulation of 15-5PH H900 steel was performed with Abaqus software to demonstrate the similarity and confidence of the numerical model. Plastic behavior was included in this FEM study, with a tabular approximation of the tensile test results (see Fig. 17) and an isotropic-kinematic hardening model. Experimental small punch tests were performed with four UL cycles initiated at 0.1, 0.2, 0.3 and 0.4 mm of punch displacement. Fig. 18 represents a comparison between the experimental and FEM simulation of the small punch test for 15-5 PH H900. The numerical SPT curve matched experimental results, so it confirmed the fit of the FEM model. Figures 19 and 20 show the remaining experimental SPT curves.

Criteria to obtain the slope of each UL cycle was the same applied in previous FEM analysis. Table 7 summarizes the slopes of all the UL cycles initiated at about 0.1 mm of punch displacement. Figure 21 shows the slope of the UL cycle initiated at 0.1 mm of punch displacement versus the elastic modulus E of each material obtained from the tensile tests. The linear regression for these data show an experimental correlation factor equal to $\lambda_{UL\_0.1}= 14.326\ mm^{-1}$, near the correlation factor obtained from the previous FEM study ($\lambda^{FEM}_{UL\_0.1}= 14.828\ mm^{-1}$; deviation of 3.6%).

This dissimilarity between both factors is originated in simplifications assumed in the FEM model (punch sphere and dies are considered as rigid bodies, fabrication tolerances generates little differences in dimensions of real and simulated SPT components, etc.).

Table 7 shows the elastic modulus obtained from UL cycles using both correlation factors ($\lambda^{FEM}_{UL\_0.1}= 14.828\ mm^{-1}$ and $\lambda_{UL\_0.1}= 14.326\ mm^{-1}$). Deviations in the elastic modulus calculation reach values of 9.06% when the FEM calculated correlation factor $\lambda^{FEM}_{UL\_0.1}= 14.828\ mm^{-1}$ is used. These deviations are reduced to 5.37% when the correlation factor is directly obtained from a linear regression of experimental tests ($\lambda_{UL\_0.1}= 14.326\ mm^{-1}$). The high level of accuracy needed in the dimensions of the punch sphere, upper and lower dies and other adjustments of the small punch test setup shows that a calibration test is needed to guarantee the highest level of accuracy in the SPT results. Although a numerical model of SPT shows enough approximation to real SPT behavior, each SPT setup should be tested with a set of materials with dissimilar elastic modulus to obtain a more accurate correlation factor $\lambda_{UL\_0.1}$ for the elastic modulus calculation. In the particular case of the experimental setup used in this investigation, the correlation factor was equal to $\lambda_{UL\_0.1}= 14.326\ mm^{-1}$, showing a good fit with numerically obtained correlation factor $\lambda^{FEM}_{UL\_0.1}= 14.828\ mm^{-1}$ as well.

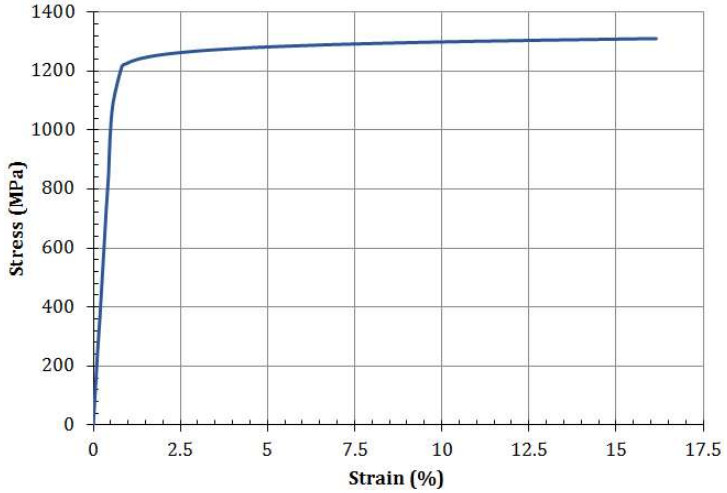

Fig. 17. Stress-strain curve of 15-5PH H900 tensile test

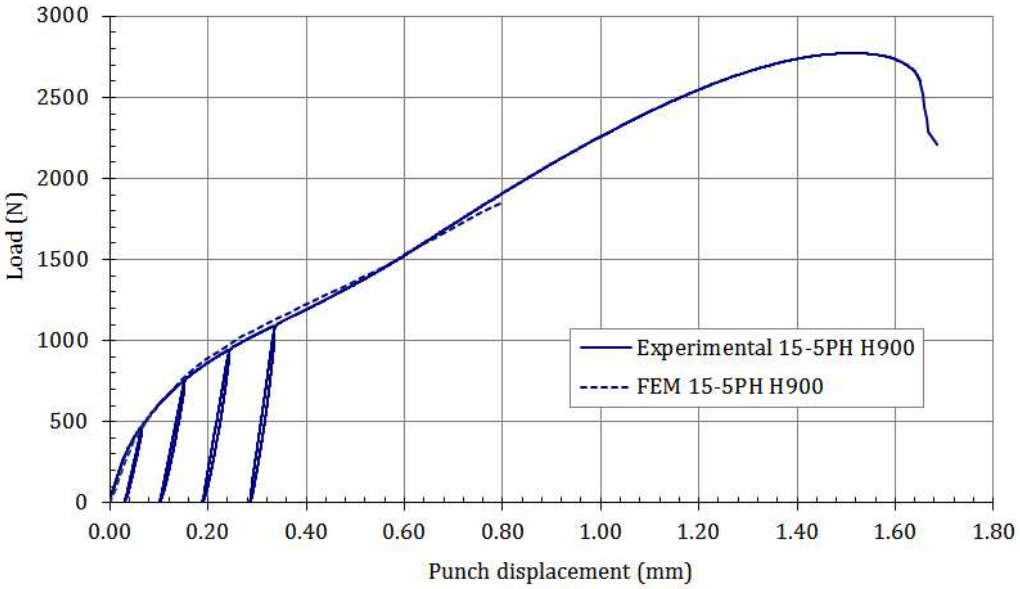

Fig. 18. Small punch tests for 15-5 PH H900 (numerical and experimental test)

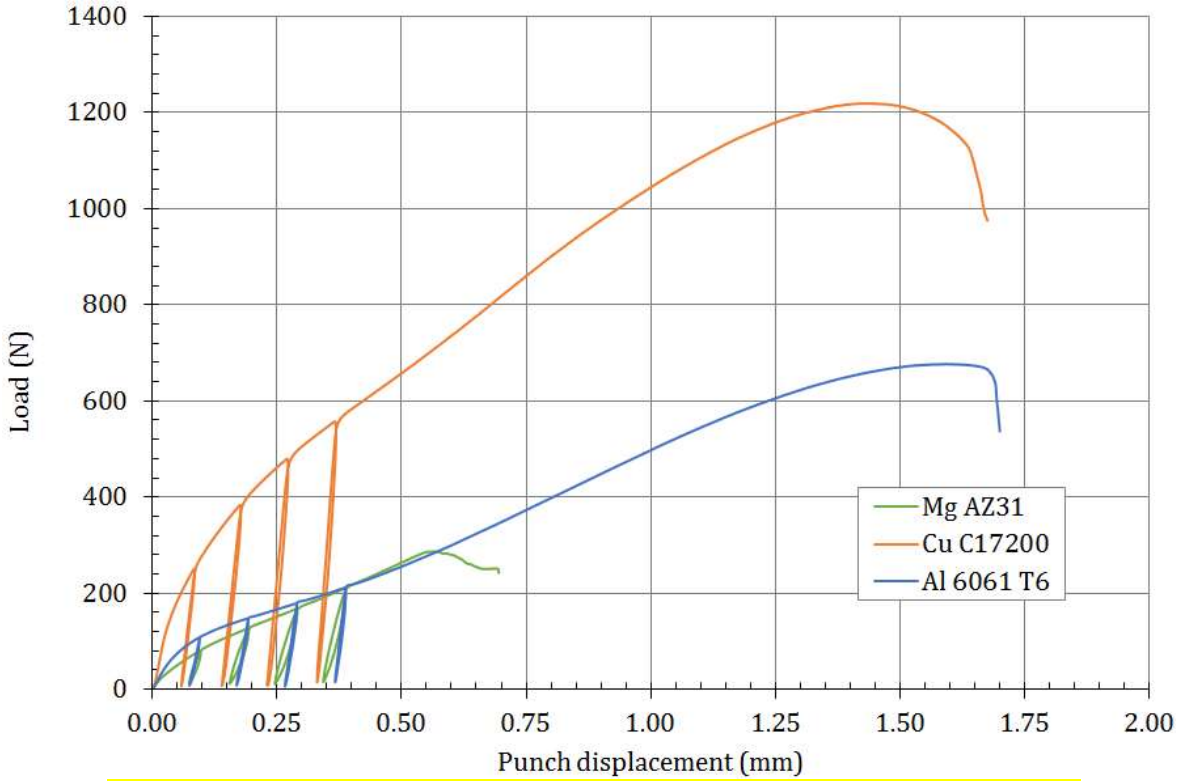

Fig. 19. Small punch tests for Al 6061 T6, Cu C18070 and Mg AZ31 alloys

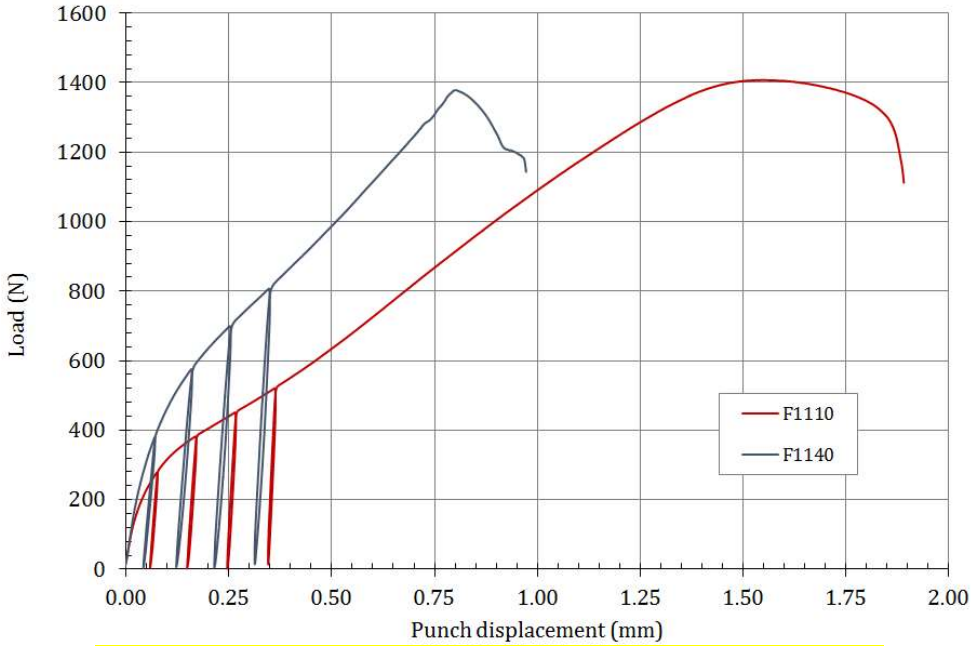

Fig. 20. Small punch tests for F1110 and F1140 carbon steels

Material	$Slope_{UL\ cycle}$ (N/mm)	$E_{tensile\ test}$ (MPa)	E_{calc_exp} (MPa)	Deviation (%)	E_{calc_FEM} (MPa)	Deviation (%)
F1110	15072.0	216430	215921.5	-0.23	223487.6	3.26
F1140	14633.0	204910	209632.4	2.30	216978.1	5.89
Al 6061 T6	4530.7	66295	64906.8	-2.09	67181.2	1.34
Mg AZ31	3154.5	42889	45191.4	5.37	46774.9	9.06
15-5PH H900	13346.0	194926	191194.8	-1.91	197894.5	1.52
Cu C18070	8854.3	128324	126846.7	-1.08	131973.3	2.92

$E_{tensile\ test}$: elastic modulus obtained experimentally from tensile tests.
E_{calc_exp}: elastic modulus obtained from correlation with $\lambda = 14.326\ mm^{-1}$.
E_{calc_FEM}: elastic modulus obtained from correlation with $\lambda = 14.828\ mm^{-1}$.

Table 7. Slopes of the experimental UL cycles and elastic modulus correlation

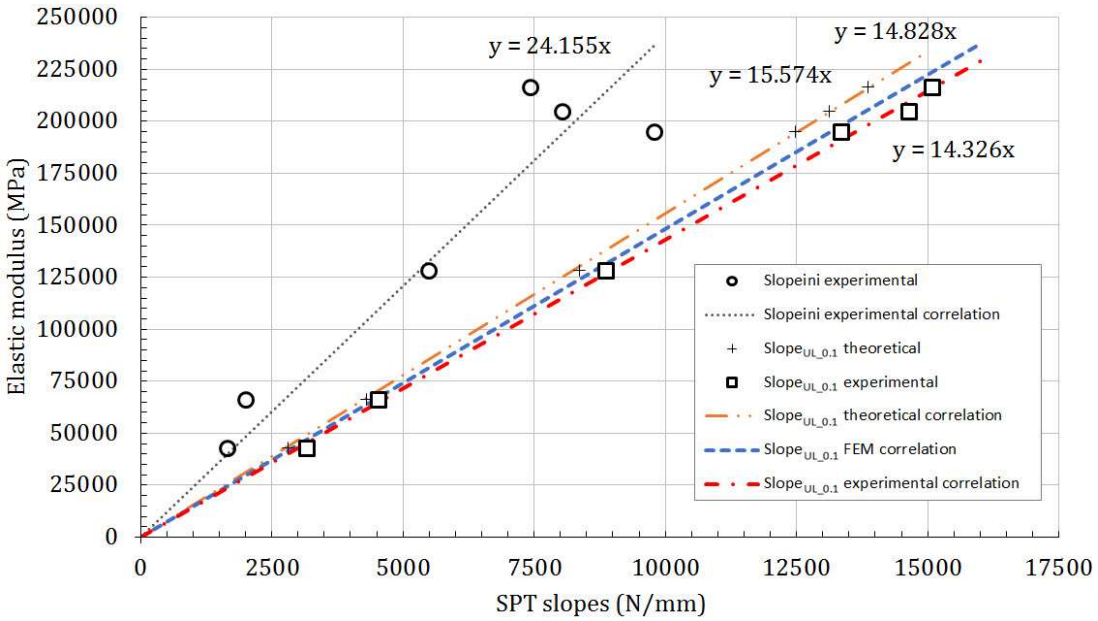

Fig. 21. Correlation between SPT slopes and the elastic modulus of the tested materials

Figure 21 shows experimental $Slope_{ini}$ for the tested materials and its correlation factor ($\lambda_{Slopeini}$ = *24.155 mm*$^{-1}$). Deviations with linear regressions were much lower in $Slope_{UL\_0.1}$ than $Slope_{ini}$.

$Slope^{Th}_{UL\_0.1}$ for each experimental material was obtained by means of Equation 18 for the theoretical model, replacing E and ν values with the data in table 1. Table 8 summarizes all of these theoretical slopes, and they are compared with experimental $Slope_{UL\_0.1}$. Figure 21 also includes a linear regression of theoretical $Slope^{Th}_{UL\_0.1}$ shown in Table 8 calculating its theoretical correlation factor ($\lambda^{Th}_{UL\_0.1}$ = *15.574 mm*$^{-1}$).

Material	$Slope^{Th}_{UL\_0.1}$ (N/mm)	Deviation (%)
F1110	13857.67	-8.06
F1140	13120.06	-10.34
Al 6061 T6	4303.07	-5.02
Mg AZ31	2812.21	-10.85
15-5PH H900	12480.80	-6.48
Cu C18070	8364.82	-5.53

$Slope^{Th}_{UL\_0.1}$: $Slope_{UL\_0.1}$ obtained with the theoretical model

Table 8. Slopes of the theoretical model and deviations with experimental $Slope_{UL\_Cycle}$

5 Conclusions

A new and improved correlation for elastic modulus prediction of isotropic and homogeneous metallic materials in the Small Punch Test has been established after a FEM calculation, a theoretical analysis, and an experimental study.

This correlation shows great accuracy for obtaining the elastic modulus E. The correlation factor λ is independent of the material plastic properties and is only related to geometrical data of the test. Considering that SPT geometrical data tends towards the standardization, a list of correlation factors λ could be established for the most common geometries of punch, dies, and specimens.

For specimens with a thickness of 0.5 mm, a lower die with an inner diameter of 4.0 mm and a fillet radius of 0.5 mm, and a punch diameter of 2.5 mm, the correlation factor $\lambda^{FEM}_{UL\_0.1}$ calculated numerically was equal to $\lambda^{FEM}_{UL\_0.1}$ = *14.828 mm*$^{-1}$. For the SPT setup used in this paper, the experimental correlation factor for the elastic modulus calculation was equal to $\lambda_{UL\_0.1}$ = *14.326 mm*$^{-1}$. Although both λ values are similar (a mismatch of 3.5%), FEM analyses showed its limitations for achieving the greatest possible accuracy. Setups with different geometries will have different correlations factors λ, and setups with the same geometry will show the same correlation factor λ.

6 References

[1] G.E. Lucas, A. Okada, M. Kiritani, Parametric Analysis of the Disc Bend Test, Journal of Nuclear Materials 141-143 (1986) 532-535. DOI: 10.1016/S0022-3115(86)80096-4

[2] G.E. Lucas, Review of Small Specimen Test Techniques for Irradiation Testing, Metallurgical Transactions A 21A (1990) 1105-1119. DOI: 10.1007/BF02698242

[3] J.M. Baik, J. Kameda, O. Buck, Development of Small Punch Tests for Ductile-brittle Transition Temperature Measurement of Temper Embrittlement Ni-Cr Steels, ASTM STP 888 (1986) 92-111. DOI: 10.1520/STP32997S

[4] X. Mao, H. Takahashi, Development of a further-miniaturized specimen of 3 mm diameter for tem disk small punch tests, Journal of Nuclear Materials 150 (1987) 42-52. DOI: 10.1016/0022-3115(87)90092-4

[5] T. Misawa, T. Adachi, M. Saito, Y. Hamaguchi, Small punch tests for evaluating ductile-brittle transition behavior of irradiated ferritic steels, Journal of Nuclear Materials 150 (1987) 194-202. DOI: 10.1016/0022-3115(87)90075-4

[6] X. Mao, M. Saito, H. Takahashi, Small punch test to predict ductile fracture toughness JIc and brittle fracture toughness KIc, Scripta Metallurgica et Materialia 25 (1991) 2481-2485. DOI: 10.1016/0956-716X(91)90053-4

[7] X. Mao, H. Takahashi, T. Kodaira, Supersmall punch test to estimate fracture toughness JIc and its application to radiation embrittlement of 21/4Cr-1Mo steel, Materials Science and Engineering AI50 (1992) 231-236. DOI: 10.1016/0921-5093(92)90116-i

[8] G.E. Lucas, The development of small specimen mechanical test techniques, Journal of Nuclear Materials 117 (1983) 327-339. DOI: 10.1016/0022-3115(83)90041-7

[9] M.P. Manahan, A.S. Argon, O.K. Harling, The development of a miniaturized disk bend test for the determination of postirradiation mechanical properties, Journal of Nuclear Materials 103 & 104 (1981) 1545-1550. DOI: 10.1016/0022-3115(82)90820-0

[10] M. Abendroth, M. Kuna, Determination of deformation and failure properties of ductile materials by means of the small punch test and neural networks, Computational Materials Science 28 (2003) 633-644. DOI: 10.1016/j.commatsci.2003.08.031

[11] T.E. García, C. Rodríguez, F.J. Belzunce, C. Suárez, Estimation of the mechanical properties of metallic materials by means of the small punch test, Journal of Alloys and Compounds 582 (2014) 708-717. DOI: 10.1016/j.jallcom.2013.08.009

[12] I.I. Cuesta, C. Rodríguez, T.E. García, J.M. Alegre, Effect of confinement level on mechanical behavior using the small punch test, Engineering Failure Analysis 58 (2015) 206-211. DOI: 10.1016/j.engfailanal.2015.09.008

[13] E. Fleury, J.S. Ha, Small punch tests to estimate the mechanical properties of steels for steam power plant: I. Mechanical strength, International Journal of Pressure Vessels and Piping 75 (1998) 699-706. DOI: 10.1016/S0308-0161(98)00074-X

[14] E.N. Campitelli, P. Spätig, R. Bonadé, W. Hoffelner, M. Victoria, Assessment of the constitutive properties from small ball punch test: experiment and modeling, Journal of Nuclear Materials 335 (2004) 366-378. DOI: 10.1016/j.jnucmat.2004.07.052

[15] T. Linse, M. Kuna, J. Schuhknecht, H.-W. Viehrig, Usage of the small-punch-test for the characterization of reactor vessel steels in the brittle-ductile transition region, Engineering Fracture Mechanics 75 (2008) 3520-3533. DOI: 10.1016/j.engfracmech.2007.03.047

[16] M.F. Moreno, G. Bertolino, A. Yawny, The significance of specimen displacement definition on the mechanical properties derived from Small Punch Test, Materials and Design 95 (2016) 623-631. DOI: 10.1016/j.matdes.2016.01.148

[17] W. Ramberg, W.R. Osgood, Description of stress-strain curves by three parameters, Technical Note 902, NACA, Washington DC, 1943.

[18] ASME, Boiler Pressure and Vessel Code, Section II, Part D, 2015.

[19] FAA, Metallic Materials Properties Development and Standardization, Edition 11, 2016.

[20] S. Timoshenko, Theory of Plates and Shells, McGraw-Hill, 1959.

[21] C. Liu, E.D. Case, Effect of Indenter Tip Radius on the Load Deflection Behavior of Thin Plates, Experimental Mechanics 37 (1997) 175-181. DOI: 10.1007/BF02317856

[22] K.L. Johnson, Contact Mechanics, Cambridge University Press, 1985. DOI: 10.1017/CBO9781139171731

[23] CEN Workshop Agreement, CWA 15627:2007 D/E/F, Small Punch Test Method for Metallic Materials, CEN, Brussels Belgium, 2007.